Communications in Physics, Vol. 34, No. 3 (2024), pp. 287-296
DOI: https://doi.org/10.15625/0868-3166/19565

Optimization of NdFeB alloy composition for preparing high-performance melt-spun ribbons

Nguyen Xuan Truong[1,2], **Vu Hong Ky**[1], **Vuong Kha Anh**[1,2], **Nguyen Hoai Nam**[1], **Dang Thi Thuy Ngan**[1], **Nguyen Huy Hoang**[1], **Nguyen Van Vuong**[1,†]

[1]*Institute of Materials Science, Vietnam Academy of Science and Technology, 18 Hoang Quoc Viet Road, Cau Giay District, Hanoi, Vietnam*

[2]*Graduate University of Science and Technology, Vietnam Academy of Science and Technology, 18 Hoang Quoc Viet Road, Cau Giay District, Hanoi, Vietnam*

E-mail: †vuongnv@ims.vast.ac.vn

Received 4 December 2023; *Accepted for publication 22 August 2024*
Published 10 September 2024

Abstract. *The magnetic field assisted melt-spinning method is a novel approach for producing anisotropic NdFeB-based ribbons and anisotropic bonded magnets. These anisotropic ribbons are required to be grown on the magnetized seeds, so the initial composition of the alloys used for melt-spinning ribbons is very crucial in creating ribbons' textured microstructures. This paper reveals the results concerning the choice of alloy compositions containing Nd, Fe, Co and B to optimize the processing of ribbons with the high texture degree, high spontaneous magnetization, large coercivity as well the strong exchange-coupling interaction. The guides of producing these ribbons are presented in detail that are fruitful in a massive production of high-performance NdFeB-based anisotropic ribbons and magnets prepared thereof.*

Keywords: NdFeCoB-based alloy composition; melt-spinning ribbons; magnetic properties.
Classification numbers: 75.50.Ww; 75.30.Gw; 75.50.Bb; 81.20.Ev; 81.20.Vj.

1. Introduction

The magnet market is characterized by the growth rate of 8.8% per year, from 14.9 billion in 2016 to 22.6 billion USD in 2021 associated with the growth of the auto industry in the Asia-Pacific region [1]. In comparison with sintered magnets (SM), the bonded magnets (BM) are of lower performance since to cede the volume of grain boundary regions to a binder, but they always

are preferred in many applications due to their easy and precise shaping, low cost and large production capacity. BMs will compete strongly with SMs once their magnetic performance should be improved.

Up to now, NdFeB-based magnets still are dominant in permanent magnet applications [2] with the energy product $(BH)_{max}$ commonly around ≤ 50 MGOe for anisotropic SMs; ≤ 20 MGOe and ≤ 10 MGOe for in-mold compacted anisotropic and isotropic BMs, respectively. NdFeB BMs made by the injection molding as well the calendering and extrusion methods own $(BH)_{max} \leq 7$ MGOe [3]. The additively 3D-printed anisotropic NdFeB BMs of 8.7 MGOe [4, 5] show a new trend of developing mass-scale of producing BMs.

Because of the phase diagram complexity [6], NdFeB-based magnets are produced by means of the powder metallurgy method. The magnet performance depends on the intrinsic properties of materials (the spontaneous magnetization M_{sp} and the magneto-crystalline anisotropy energy K_a) and the extrinsic ones like the alignment of easy axes of particles inside magnets (the magnet texture), the magnet microstructure including grain size distributions, grain shapes and magnet mass density values.

For a large-scale production of NdFeB-based magnets, it is very convenient to use melt-spun ribbons since the rapid quench state of the melt-spinning technology allows to avoid difficulties in forming the phase $Nd_2Fe_{14}B$ caused by the phase diagram complexity of NdFeB systems. However, the conventional melt-spinning technology can produce only isotropic ribbons since the crystalline growth of ribbons is derived by the undercooling temperature gradient ΔT appeared on the wheel surface of a spinner for very short time, so the crystal growth is non-equilibrium and thus leads to the poor directional growth of ribbons. So, the melt-spun ribbons contain grains with their easy axes oriented randomly over the ribbon volume and thus causes their isotropic feature.

The magnetic field assisted melt-spinning (MFAMS) technology crucially changes the mechanism of ribbon formation. The presence of external magnetic fields contributes to the driving force of crystalline growth process improving the directional crystalline growth and thus allows to form anisotropic ribbons.

In the previous work [7, 8], it has been noted that, to form MFAMS ribbons the prerequisite requirement is the presence of seeds which can be magnetized in an external magnetic field. In the case of NdFeB-based systems, the soft ferromagnetic element Fe plays the role of these seeds and the starting composition of alloys used in melt-spinning experiments is very important for preparing high performance anisotropic ribbons. The fraction of ferromagnetic elements in NdFeB-based alloys must be kept optimal for supplying the ferromagnetic seed amount to stimulate the ribbon formation in an assisted magnetic field and to control the ribbons' compositions around the $Nd_2Fe_{14}B$ phase as well the possible exchange coupling between the hard and soft phases appeared in the final ribbon products. This problem has been solved and discussed in detail in this paper.

2. Experiment

The commercial melt-spinner ZGK-1 has been used for quenching NdFeB-based alloys into ribbons. The alloy batch contained high purity elements 4N grade of Nd, Fe, Co and B weighted at 20 gram in desired mass ratios and was arc-melted thrice to ensure high homogeneity. The arc-melted alloys were divided into approximately 5 gram pieces per batch for melt-spinning experiments. The spinner's chamber was filled by 0.8 atm argon gas after 5-fold cleaning by

means of argon flows controlled by a vacuum pump. The loaded alloy amount was induction-melted and ejected thru the 2mm-diameter-orifice onto the surface of the wheel which stays at 3mm distance away from the orifice and rotating with different tangent speeds in the range of 5 ÷ 25 m/s. The phase determination of ribbons was done by using the Rietveld refinement of X-ray diffraction (XRD) patterns of ribbon pulverized samples. The texture of ribbons was also observed and estimated by analyzing the peak set of XRD patterns taken on the ribbon flake surfaces. The ribbons magnetic characteristics were estimated by considering their hysteresis loops measured by the VSM as well the SQUID magnetometer.

3. Results

3.1. $Nd_{15}Fe_{77}B_8$ starting alloy composition

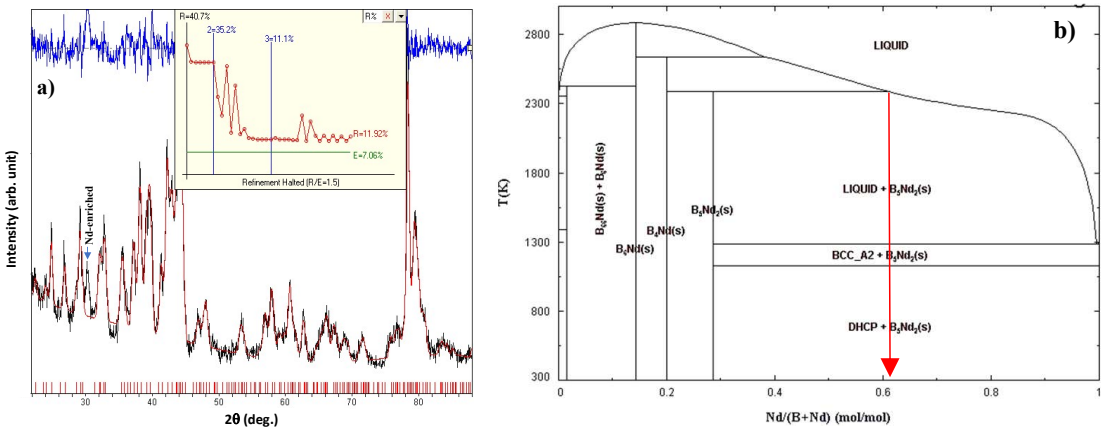

Fig. 1. (a) The Rietveld refinement matching the calculated (red curve) and observed (black curve) the XRD pattern of the powder ground from ribbons melt-spun at 15.8 m/s using the starting alloy $Nd_{15}Fe_{77}B_8$. (b) The peak appeared at 30.25° corresponds to the phase $Nd_4B_{2.5}$ which is rapidly quenched along the red arrow indicated on the sketched Nd-B binary phase diagram taken from [9].

It is well known that, the high-performance sintered NdFeB magnets are produced by using the starting alloys of the composition $Nd_{15}Fe_{77}B_8$. This composition is featured by the Nd-enrichment that enhances the coercivity caused by the Nd-rich layers on the grain boundaries. This alloy has been also taken into account for melt-spinning ribbons. The ribbons were finely produced with the averaged thickness of 20 μm and the length of several centimeters. Based on the material conservation rule we have $Nd_{15}Fe_{77}B_8 = 5.5\cdot$ ($Nd_2Fe_{14}B$) + $Nd_4B_{2.5}$ leading to the XRD pattern of the ribbon ground powder as plotted in Fig. 1. The stoichiometric phase $Nd_2Fe_{14}B$ is thermodynamically favored in solidifying of $Nd_{15}Fe_{77}B_8$ system even in the great undercooling state, the rest Nd and B can be solidified along the arrow indicated on the Nd-B phase diagram shown in the right side of Fig. 1. This phase is enriched in Nd and appeared on the XRD pattern by the peak at about $2\theta = 30.25°$. This Nd-enriched phase stays at the grain boundaries and plays the role of pinning centers and just enhances the ribbon coercivity while the great fraction of $Nd_2Fe_{14}B$ matrix determines the ribbon spontaneous magnetization M_{sp} and consequently, the

saturation magnetization M_{sat}. These two factors of coercivity and magnetization are decisive in establishing a good magnetic performance of ribbons and they are reasonable why the composition of $Nd_{15}Fe_{77}B_8$ has been chosen as the most suitable for preparing the high-performance sintered magnets as well the melt-spun ribbons.

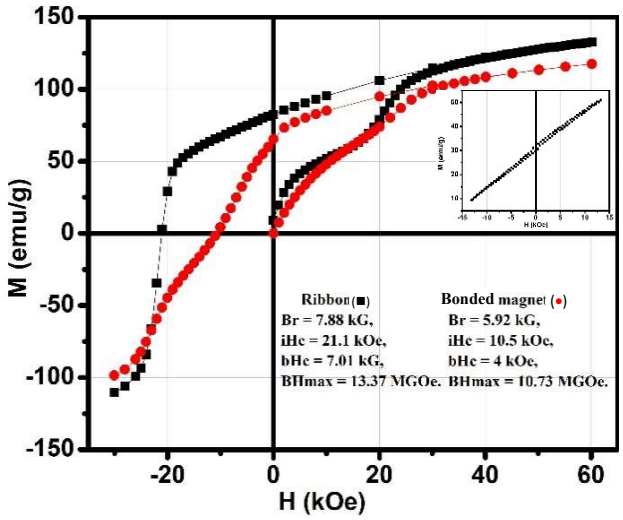

Fig. 2. The room temperature SQUID magnetization loops of the ribbons melt-spun at 15.8 m/s using the starting alloy $Nd_{15}Fe_{77}B_8$ (■) and the bonded magnet prepared using the powder ground from these ribbons (•). The sketch shows the VSM magnetization loop of the ribbon sample.

Figure 2 shows the hysteresis loop of the ribbon melt-spun at 15.8 m/s using the starting alloy of $Nd_{15}Fe_{77}B_8$. The square dotted curve is the loop of the ribbon. Since the ribbon is isotropic, so the remanence magnetization M_r = 7.88 kG is around a half of M_{sp} = 16.1 kG [10] for the $Nd_2Fe_{14}B$ system. The presence of a Nd-enriched phase on the grain boundaries is characterized by the knee appeared on the initial magnetization curve at about H = 18 kOe which is the fact that Nd excess atoms play as pinning centers leading to the large coercivity ${}_iH_c$ = 21.1 kOe of ribbons. The high coercivity value is the distinguish feature of the prepared ribbons causing the non-adequate loop measurement using the VSM at the maximal magnetizing field of about 10 kOe as shown in the figure sketched on Fig. 2. Once ribbons are isotropic, their energy product $(BH)_{max}$ is 13.37 MGOe, around 83% of the theoretical value $(M_{sp}/2)^2/4$ = 16.2 MGOe for the isotropic $Nd_2Fe_{14}B$ system.

The obtained ribbons were used for preparing bonded magnets. The ribbons were high-energy ball-milled for 5 min. in the protective environment of xylene, dried in a glove box and impregnated with the PPS (Polyphenylene Sulfide) binder. The dried impregnated powders were in-mold compacted under 5000 psi pressure and cured into solid magnet at 180°C. The magnet density was 7.2 g/cm^3, about 94% of that for ribbons (7.6 g/cm^3). It is understood, that the bonded magnet consists of the randomly compacted particles so the magnet's microstructure is less ordered than that of ribbons, so although the knee is appeared again on the initial magnetization curve indicating that Nd phase stays on the grain boundaries, but the less ordered microstructure

decreases the magnet coercivity ${}_{\mathrm{i}}\mathrm{H}_{\mathrm{c}}$ down to 4 kOe compared with 7.01 kOe of ribbons. So totally, $(\mathrm{BH})_{\mathrm{max}}$ of the obtained magnet is only 10.73 MGOe, about 80% of the energy product value of ribbons. It is worthy here to note, that anyway the announced value is good for applications of bonded magnets.

3.2. $Nd_2Fe_{14}B$ starting alloy composition

As above mentioned, the phase of $\mathrm{Nd_2Fe_{14}B}$ is the main ferromagnetic phase of Nd-Fe-B system. This stoichiometric composition is instantly formed even the starting alloy for melt-spinning is $\mathrm{Nd_{15}Fe_{77}B_8}$. Now one considers what happens if the starting alloy is stoichiometric. The alloy of $\mathrm{Nd_2Fe_{14}B}$ was prepared by using Nd, Fe, B of 4N-grade purity. The alloy was arc-melted thrice for homogeneity. The ribbon was melt-spun with the same conditions used for the above presented ribbons. Fig. 3 presents the XRD patterns of the ribbon flake contact and free surfaces (the ribbon surface contacting and non-contacting with the wheel surface). The patterns show the peak set of the pure phase $\mathrm{Nd_2Fe_{14}B}$ with the weak texture on the contact surface and very strong texture on the free surface. These phenomena correspond to the impact of the driving force of the great temperature gradient ΔT perpendicular to the wheel surface. This ΔT is caused by the great heat absorption of the wheel in comparison to the heat contained in the molten alloy flow ejected thru the nozzle orifice.

To quantify the ribbon texture degree, one uses the ratio γ between the intensities of the peaks (006) and (410), $\gamma = I_{(006)}/\mathrm{I}_{(410)}$. Since the former represents the crystalline C-axis (00l) while the latter represents the basal surface (hk0). To obviously observe the change of texture degrees on the two surfaces of ribbons, the peaks (410) and (006) appeared in the range of $2\theta = 42.5 \div 45.5^{\circ}$ are illustrated in the sketch of Fig. 3.

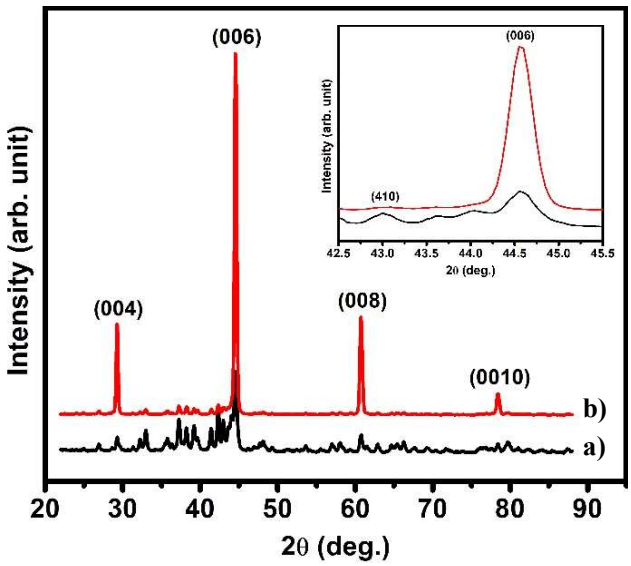

Fig. 3. The XRD patterns of the contact (a) and free (b) surfaces for the $\mathrm{Nd_2Fe_{14}B}$ ribbon melt-spun at 15.8 m/s wheel speed.

The texture degree γ of the contact surface is 3.5 and increased up to 50 for the free surface. One understands that, the ribbon's texture causes its anisotropy, but the mentioned texture inhomogeneity of ribbons prepared by this conventional melt-spinning technique causes the poor texture for magnets manufactured thereof.

Owning the stochiometric phase of $Nd_2Fe_{14}B$ but losing the grain boundary Nd-enriched phase, in comparison with the ribbons prepared from the starting $Nd_{15}Fe_{77}B_8$ alloy, the ribbons melt-spun from $Nd_2Fe_{14}B$ alloy should have a high M_{sp} (and M_{sat}) but low ${}_iH_c$. This fact is seen on the Fig. 4 with the magnetization loop M(H) measured for the prepared ribbon flake. The magnetization measured at 60 kOe is 15.1 kG, about 94% of M_{sp} of $Nd_2Fe_{14}B$ phase, but the coercivity ${}_iH_c$ is low, equals only 2 kOe leading to the small value of $(BH)_{max}$.

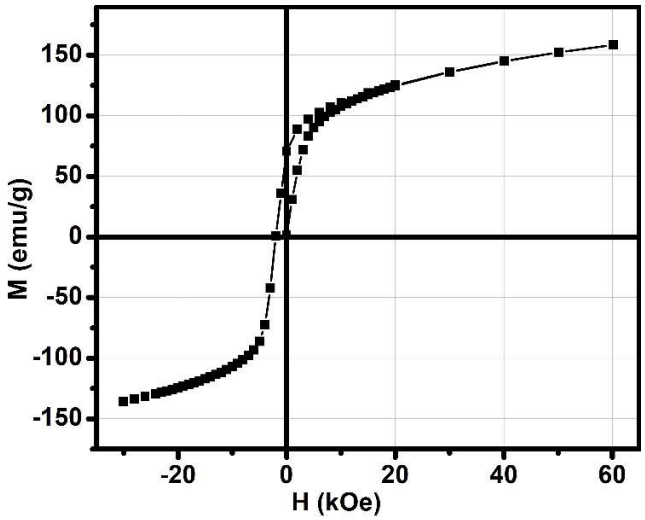

Fig. 4. The room temperature magnetization loop of the ribbon melt-spun from the starting $Nd_2Fe_{14}B$ alloy at 15.8 m/s wheel speed.

3.3. $Nd_{2.33}(Fe_{0.93}Co_{0.07})_{15}B$ starting alloy composition

To combine the advantages in the large coercivity and high magnetization of the starting alloy compositions of $Nd_{15}Fe_{77}B_8$ and $Nd_2Fe_{14}B$ presented above, the composition $Nd_{2.33}(Fe_{0.93}Co_{0.07})_{15}B$ is suggested to be prepared. This composition includes the Nd enrichment to keep coercivity high and the addition of some percent of Cobalt to Fe in order to increase the spontaneous magnetization as well the Curie temperature T_c. Compared with the stochiometric composition of $Nd_2Fe_{14}B$, this composition is Nd-enriched to control the coercivity and enriched in the 3d elements Fe and Co to increase the spontaneous magnetization through the exchange coupling interaction. Especially, the Co element is added to cause the ribbon thermal stability because of its high Curie temperature (1115 ˚C in comparison with 770 ˚C of Fe) [11].

The XRD patterns of ribbon flakes plotted on Fig. 5 show the main phase of $Nd_2Fe_{14}B$ with the weak texture degrees, $\gamma = 0.88$ and 1.13 for the contact and free surfaces, respectively. These low values of γ reveal that the crystal growth of this kind of ribbons was not intensive in comparison with the case of the $Nd_2Fe_{14}B$ alloy composition.

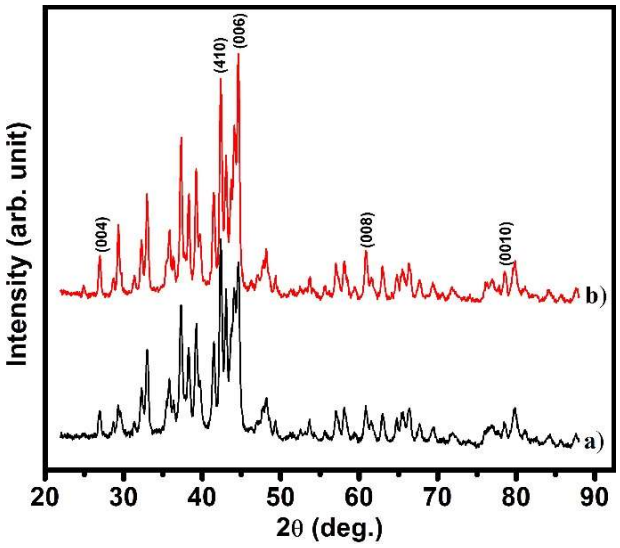

Fig. 5. The XRD patterns of the contact (a) and free surfaces (b) of the ribbon melt-spun from the starting $Nd_{2.33}(Fe_{0.93}Co_{0.07})_{15}B$ alloy at 15.8 m/s wheel speed.

The magnetic performance of the powder ground from this kind of this ribbon is estimated by its magnetization loop presented in Fig. 6. With the ribbon's density of 7.6 g/cm^3, the remanence B_r reaches 9.04 kG, $_iH_c$ is improved (compared with the value of 2 kOe of the ribbon melt-spun from $Nd_2Fe_{14}B$ alloy) to 7.05 kOe, $_bH_c$ = 5.9 kOe and $(BH)_{max}$ is 15.05 MGOe.

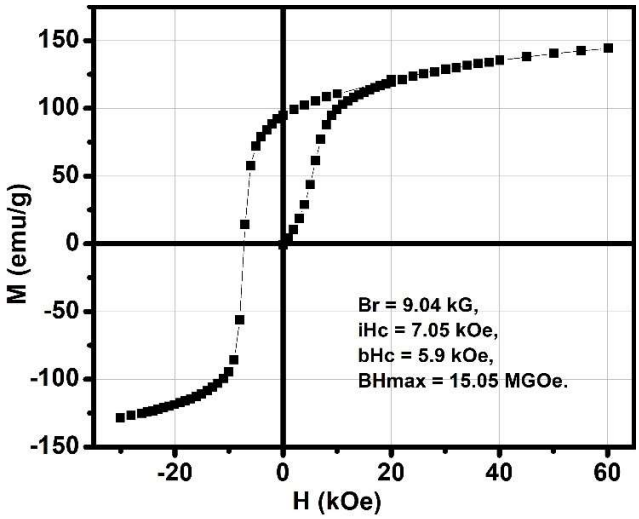

Fig. 6. The room temperature magnetization loop of the ground ribbon melt-spun at 15.8 m/s wheel speed using the starting $Nd_{2.33}(Fe_{0.93}Co_{0.07})_{15}B$ alloy.

3.4. $Nd_{2.33}(Fe_{0.93}Co_{0.07})_{18.5}B$ starting alloy composition

This composition has been chosen with keeping the ordinary enrichment of Nd. But the fraction of $Fe_{0.93}Co_{0.07}$ is further increased to test the exchange coupling between hard and soft phases following the theory of Kneller and Hawig [12] for the nanostructured nanocomposite microstructure of ribbons. The ribbons coercivity can be also controlled by a larger wheel speed to reduce the grain sizes.

The starting alloy $Nd_{2.33}(Fe_{0.93}Co_{0.07})_{18.5}B$ was arc-melted and ejected into ribbons at different wheel speeds in the range of 15.8 – 25 m/s. Other parameters of the melt-spinning process are the same as used for the above discussed ribbons. It is observed that the wheel speeds and in turn, the cooling rates, effect significantly on the magnetic properties. As shown by the loops plotted on the Fig. 7, the optimal wheel speed is 18 m/s. This speed is larger than that of 15.8 m/s for ribbons melt-spun using either $Nd_{15}Fe_{77}B_8$ or $Nd_2Fe_{14}B$ starting alloys. With again the ribbon mass density of 7.6 g/cm^3, the magnetic properties of this best ribbon are B_r = 9.9 kG, $_iH_c$ = 6.5 kOe, $_bH_c$ = 5.01 kOe and $(BH)_{max}$ = 13.3 MGOe.

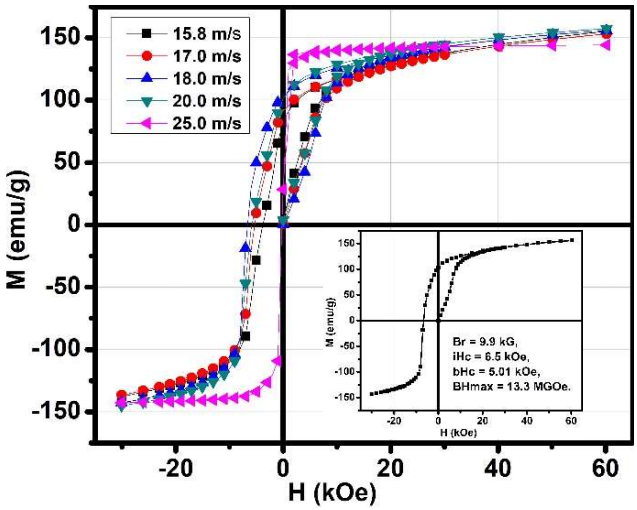

Fig. 7. The room temperature magnetization loop of the ribbons melt-spun from the starting $Nd_{2.33}(Fe_{0.93}Co_{0.07})_{18.5}B$ alloy at different wheel speeds. The sketch shows the loops of the best ribbon melt-spun at 18 m/s wheel speed.

Corresponding to these loops, the XRD patterns (see Fig. 8) also strongly depend on the wheel speeds. The peaks stay belonging to the phase of $Nd_2Fe_{14}B$, but the texture degree γ changes significantly, γ increases from 1.78 to 2.75 but decreases down to 2.19, 0.81 and 0.11 for ribbons melt-spun at 15.8, 17, 18, 20 and 25 m/s, respectively. This phenomenon proves that the thermal state of the ribbon solidification complicatedly depends on the wheel speed. The undercooling temperature is almost constant and equals the difference between the alloy melting temperature and the room temperature of the big-mass wheel. The temperature gradient ΔT plays the main driving force of ribbon solidification, and the direction of this gradient is perpendicular to the wheel surface if the wheel speed is small ($\leq$ 17 m/s for the melt-spinner used in this paper) and

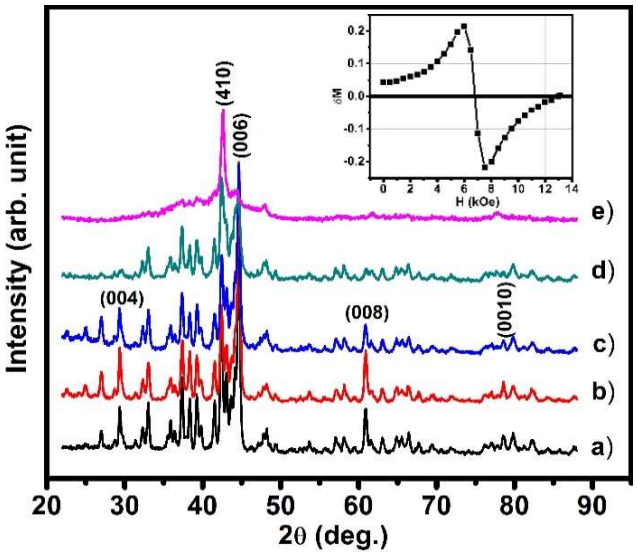

Fig. 8. The XRD patterns of the flake free surfaces of ribbons $Nd_{2.33}(Fe_{0.93}Co_{0.07})_{18.5}B$ melt-spun at 15 (a), 17 (b), 18 (c), 20 (d) and 25 m/s (e) wheel speeds. The (00l) peaks and the strongest peak (410) of $Nd_2Fe_{14}B$ phase are indicated. The sketch is the Henkel plot of the ribbon melt-spun at 18 m/s

changes to tangential for larger speeds. For example, the peak (006) disappears on the flake surface of the ribbon melt-spun at 25 m/s, while the peak (410) representing the unit cell basal plan becomes dominating. This effect is the reasons why the loop of the ribbon melt-spun at 25 m/s is characterized by both small values of ${}_iH_c$ and M_s measured at 60 kOe (see Fig. 7).

The alloy $Nd_{2.33}(Fe_{0.93}Co_{0.07})_{18.5}B$ is enriched in 3d elements of Fe and Co. Its ribbons, therefore are high in magnetization, meanwhile the coercivity as a non-intrinsic parameter depends on the ribbon microstructure. With the excess of Fe/Co embedded in the main $Nd_2Fe_{14}B$ hard phase matrix, the exchange coupling between them can keep ${}_iH_c$ large. To check the existence of exchange coupling interaction in the ribbon melt-spun at 18 m/s, the Henkel plot [13, 14] was measured and sketched in Fig. 8.

For the non-interactive system of hard and soft phase grains, the demagnetization remanence $M_d(H)$ rightly equals $[M_r(\infty) - 2M_r(H)]$. So, the deviation from the linearity of the difference δM between these two values is accepted as the evidence for magnetic interactions existed inside the system. The initial positive δM observed in this sketch confirms the existence of ferromagnetic exchange coupling interactions between the hard and soft magnetic grains and the change in δM from the positive to negative values reveals the magnetostatic interaction in this ribbon happened at the field ge6.5 kOe.

4. Conclusions

The paper shows the obtained results and releases the experimental facts that the starting alloy compositions significantly effect on the quality of NdFeB-based melt-spun ribbons. The pure

stoichiometric composition $Nd_2Fe_{14}B$ allows to melt-spin ribbons of high spontaneous magnetization M_{sp}, large texture γ but low coercivity ${}_iH_c$. The composition $Nd_{15}Fe_{77}B_8$ can be used for melt-spin large coercivity ribbons but paid by low magnetization and texture degree. The soft phase enriched composition as $Nd_{2.33}(Fe_{0.93}Co_{0.07})_{15}B$ is recommended for melt-spinning high-quality ribbons. Moreover, it is also recommended to utilize the composition $Nd_{2.33}(Fe_{0.93}Co_{0.07})_{18.5}B$ to melt-spin high-performance nanocomposite ribbons, in which the exchange coupling exists and allows the high M_s and ${}_iH_c$ of ribbons. It is noted that, the wheel speed plays an important role in fixing the quality of ribbons and must be optimized to the chosen composition of initial alloys. With the fixed mentioned parameters of melt-spinning process, it was found that the optimal wheel speed is about 18 m/s for the nanocomposite and 15.8 m/s for other ribbons. These guidelines are useful for a mass-scale production of high-performance NdFeB-based ribbons.

Acknowledgement

This research is funded by Vietnam National Foundation for Science and Technology Development (NAFOSTED) under grant number 103.02-2021.69.

References

[1] https://www.marketsandmarkets.com/Market-Reports/permanent-magnet-market-806.html. (Access at 28/11/2023.)

[2] J. Cui, J. Ormerod, D. Parker, R. Ott, A. Palasyuk, S. Mccall, M. P. Paranthaman, M. S. Kesler, M. A. Mcguire, I. C. Nlebedim, C. Pan and T. Lograsso, *Manufacturing processes for permanent magnets: Part I—sintering and casting*, JOM **74** (2022) 1279.

[3] J. Cui, J. Ormerod, D. Parker, R. Ott, A. Palasyuk, S. Mccall, M. P. Paranthaman, M. S. Kesler, M. A. Mcguire, I. C. Nlebedim, C. Pan and T. Lograsso, *Manufacturing Processes for Permanent Magnets: Part II—Bonding and Emerging Methods*, JOM **74** (2022) 2492.

[4] K. Gandha. M. P. Paranthaman, H. Wang. X. Liu, I. C. Nlebedim, *Thermal stability of anisotropic bonded magnets prepared by additive manufacturing*, J. Am. Ceram. Soc. **106** (2023) 166.

[5] A. Grujic, D. Nedeljkovic, J. Stajic-Trosic, M. Z. Stijepovic, S. Alnouri and S. Perisic, *Magneto-Mechanical and Thermal Properties of Nd-Fe-B-Epoxy-Bonded Composite Materials*, Polymers **15** (2023) 1894.

[6] M. Sagawa, S. Fujimura, H. Yamamoto, Y. Matsuura, K. Hiraga, *Permanent magnet materials based on the rare earth-iron-boron tetragonal compounds*, IEEE Trans. Magn. **20** (1984) 1584.

[7] V. V. Nguyen, C. Rong, Y. Ding and J. P. Liu, *Effect of magnetic fields on melt-spun Nd2Fe14B-based ribbons*, J. Appl. Phys. **111** (2012) 07A731.

[8] X. T. Nguyen, H. K. Vu, H. M. Do, V. K. Nguyen, and V. V. Nguyen, *The Effect of External Magnetic Field on Microstructure and Magnetic Properties of Melt-Spun Nd-Fe-B/Fe-Co Nanocomposite Ribbons*, Adv. Mater. Sci. Eng. **2013** (2013) 927356.

[9] https://www.crct.polymtl.ca/fact/phase_diagram.php?file=B-Nd.jpg&dir=SGTE2014. (Access at 28/11/2023.)

[10] J. Fischbacher, A. Kovacs, M. Gusenbauer, H. Oezelt, L. Exl, S. Bance and T. Schrefl, *Micromagnetics of rare-earth efficient permanent magnets*, J. Phys. D: Appl. Phys. **51** (2018) 193002.

[11] P Mohn and E P Wohlfarth, *The Curie temperature of the ferromagnetic transition metals and their compounds*, J. Phys. F: Met. Phys. **17** (1987) 2421.

[12] E. F. Kneller and R. Hawig, *The Exchange-Spring Magnet: A New Material Principle for Permanent Magnets,* IEEE Trans. Magn, **27** (1991) 3588.

[13] O. Henkel, *Remanenzverhalten und Wechselwirkungen in hartmagnetischen Teilchenkollektiven,* Phys. Stat. Sol. **7** (1964) 919.

[14] A. Xia, Y. Li, T. Li, S. Su, C. Jin, X. Liu, *The availability of Henkel plots for sintered hard/soft magnetic composite ferrites,* Phys. B: Condens. Matter. **493** (2016) 14.